ORIGINAL RESEARCH

Stereotactic Comparison among Cerebral Blood Volume, Methionine Uptake, and Histopathology in Brain Glioma

N. Sadeghi
I. Salmon
C. Decaestecker
M. Levivier
T. Metens
D. Wikler
V. Denolin
S. Rorive
N. Massager
D. Baleriaux
S. Goldman

BACKGROUND AND PURPOSE: Vascularity, metabolism, and histologic grade are related in gliomas but the exact determinants of these relationships are not fully defined. We used image coregistration and stereotactic biopsies to regionally compare cerebral blood volume (CBV) and ^{11}C-methionine (MET) uptake measurements in brain gliomas and to assess their relationship by histopathologic examination.

MATERIALS AND METHODS: Fourteen patients with brain gliomas underwent MR imaging, including dynamic susceptibility contrast-enhanced MR and positron-emission tomography (PET) using MET acquired in identical stereotactic conditions before biopsy. MR-based CBV maps were calculated and both CBV maps and PET images were coregistered to anatomic images. Sixty-five biopsy samples were obtained on trajectories targeted toward high MET uptake area. The following histopathologic features were semiquantified in each sample: mitotic activity, endothelial proliferation, cellular pleomorphism, and tumor necrosis. CBV and MET uptake values were measured in the biopsy area and normalized to contralateral white matter. CBV ratios were compared with MET uptake ratios, and both measurements were compared with histologic features of each sample.

RESULTS: CBV ratios ranged from 0.08 to 10.24 (median = 1.73), and MET uptake ratios ranged from 0.30 to 4.91 (median = 1.67). There was a positive correlation between CBV ratios and MET uptake ratios ($r = 0.65$, $P < .001$). Both CBV and MET uptake ratios were found to be significantly related to endothelial proliferation and mitotic activity ($P < .01$).

CONCLUSION: Within glial tumors, there is a local relationship between CBV and MET uptake measurements. Both provide indices of focal malignant activity.

In patients with cerebral gliomas, accurate histopathologic grading is mandatory to plan treatment and to provide prognosis. Histopathologic grading is based on cellular pleomorphism, mitotic activity, endothelial cell proliferation, and tumor necrosis.[1] Because these pathologic features may be distributed heterogeneously within an individual tumor,[2] biopsy-based histopathologic examination may be advantageously guided by functional imaging to target the most malignant region.[3-7]

Positron-emission tomography (PET) with ^{11}C-methionine (MET) and dynamic susceptibility contrast-enhanced MR with cerebral blood volume (CBV) mapping are able to reflect, respectively, the amino acid metabolism and the vascularity of gliomas. As such, these techniques are used to target stereotactic biopsy.[4-7] Besides image-based biopsy targeting, MET uptake and CBV measurement inform us noninvasively on the biologic status of the entire tumor. Many studies have reported the use of PET-MET to investigate malignancy, extent of tumor spread, effectiveness of therapy, and prognosis of brain tumors.[8-12] PET-MET has been also applied for the guidance of tumor resection and radiosurgery.[13,14] More specifically, previous studies have demonstrated relationships between MET uptake and cell proliferation in cell culture,[15] Ki-67 protein expression,[16] proliferating cell nuclear antigen expression,[17] and microvessel density.[18] Thus MET-uptake may be used as an indirect marker for tumor proliferation and angiogenesis. The influence of angiogenesis on MET uptake is actually expected because the amino acid transport within the brain is dependent on the expression of transporters at the surface of the endothelium.[19,20] Angiogenesis is also expected to influence the relative volume of blood in brain tumors that is evaluated by CBV measurements. Although CBV measurements have frequently been reported as an interesting tool in grading gliomas,[21-23] we still lack details on its relationship with tumor metabolism and specific malignant features. As a measure of tissue vascularity, the relationship between maximum CBV values and both microvessel density and vascular endothelial growth factor have been investigated and showed some correlations.[24-27] Based on these data, the various degrees of neoangiogenesis that occur in gliomas may influence CBV and tumor metabolism in parallel. Indeed, Aronen et al[28] reported an association between CBV, glucose uptake, and tumor angiogenesis in gliomas. In these studies, however, image-based measurements were not obtained in the precise region of histologic sampling; maximum values of CBV measured in the whole tumor have been considered for comparison with results of histologic examination in the most representative tissue samples obtained from biopsy or resection. The high degree of heterogeneity of glial tumors renders it preferable to compare, in the same areas of the tumor, imaging measurements and histologic analysis.

To test the hypothesis that a relationship between CBV and metabolism is present at a local level within gliomas, we applied stereotactic coregistration of PET-MET, CBV mapping,

Received March 21, 2006; accepted after revision June 10.

From the Departments of Radiology (N.S., T.M., V.D., D.B.), Pathology (I.S., S.R.), Neurosurgery (M.L., D.W., N.M.), and PET/Biomedical Cyclotron Unit (D.W., S.G.), Hôpital Erasme, Brussels, Belgium; and Laboratory of Toxicology (C.D.), Université Libre de Bruxelles, Boulevard du Triomphe, Brussels, Belgium.

N.S. was supported by Fond National de la Recherche Scientifique (FNRS) and Erasme Foundation grants. C.D. is a Senior Research Associate with the FNRS, Brussels, Belgium.

Paper previously presented at: Annual Meeting of the American Society of Neuroradiology, April 29–May 5, 2006; San Diego, Calif.

Address correspondence to Niloufar Sadeghi, MD, Department of Radiology, Hôpital Erasme, 808, Route de Lennik, 1070 Brussels, Belgium; e-mail: nsadeghi@ulb.ac.be.

and high-resolution anatomic MR images to regionally compare CBV and MET uptake measurements in patients addressed for a brain tumor biopsy. This study also assesses the local relationships between these measurements and various histopathologic features, including endothelial proliferation.

Materials and Methods

Subjects

Fourteen patients, 6 men and 8 women, with a mean age of 42 years (range, 19–78 years; SD, 18), with histologically proved brain gliomas were included in the study. The histologic diagnosis was based on stereotactic biopsy in all cases. Institutional review board approval and patient written informed consent were obtained. Two patients had previously undergone surgical resection at the time of the study and presented with recurrent tumor. All other patients had no previous treatment.

MR Imaging

Before imaging, a stereotactic head frame was attached to the patient's head under local anesthesia with mild sedation. MR images including perfusion-weighted echo-planar images were acquired during the same procedure. An 18-gauge intravenous catheter was used for contrast agent administration. Imaging was performed on a 1.5T MR unit (Gyroscan NT; Philips Medical Systems, Best, the Netherlands). A standard circularly polarized head coil was used. MR brain studies consisted of sagittal and axial T1-weighted images (TR, 422 ms; TE, 9 ms; section thickness, 5 mm; FOV, 216 × 270 mm; data matrix, 256 × 256), and axial turbo spin-echo fluid-attenuated inversion recovery (FLAIR) images (TR, 6500 ms; TE, 150 ms; TI, 2200 ms; section thickness, 4 mm; FOV, 216 × 270 mm; data matrix, 256 × 256). Dynamic susceptibility-weighted contrast-enhanced MR imaging was performed during the first pass of a bolus of gadopentetate dimeglumine (Dotarem; Guerbet Laboratories, Aulnay-sous-Bois, France). Dynamic MR imaging was performed using a 3D multishot shifted-echo echo-planar MR imaging sequence (principles of echo shifting with a train of observations)[29,30] with the following parameters: effective TR 17 ms; TE, 25 ms; flip angle, 7°; FOV, 216 × 270 mm; section thickness, 3.5 mm; data matrix, 51 × 64; and in-plane acquisition voxel size, 4.22 × 4.30 mm (reconstruction: 2.11 × 2.11 mm). Thirty sections were obtained. A series of 40 multisection acquisitions was acquired at 1.9-second intervals. The first 3 acquisitions were performed before contrast agent injection to establish a precontrast baseline. At the 5th second, contrast (0.1 mmol/kg) was injected with a power injector (Spectris MR injector; MedRad, Indianola, Pa) at a rate of 5 mL/s, immediately followed by a bolus injection of saline. After dynamic contrast imaging, a high resolution, 3D dataset was acquired using a T1-weighted, spoiled gradient echo-pulse sequence (3DT1) (TE, 20 ms; TR, 4.6 ms; flip angle, 25°; section thickness, 1.3 mm; FOV, 216 × 270 mm; data matrix, 272 × 512). This dataset was used for subsequent image coregistration to the 3D PET data.

PET Imaging

After MR image acquisition, patients were transferred directly to the PET suite. All patients, who had fasted before the procedure, were injected intravenously with approximately 260 MBq of MET which was prepared according to a method adapted from Comar et al.[31] Twenty-minute emission scans were obtained starting 20 minutes after injection. Attenuation correction was performed by a transmission scan. The PET-MET was performed on an ECAT 962-HR+ operated in 3D mode (CTI-Siemens, Knoxville, Tenn). This system provided a set of 63 planes with a section thickness of 2.4 mm. Images were reconstructed by filtered back projection, displayed and analyzed using the ECAT software.

Surgery and Histopathologic Analysis

The biopsy was guided by combined stereotactic MR images and coregistered stereotactic PET images (Leksell GammaPlan software; Elekta AB, Stockholm, Sweden) as described previously.[32]

Two to 11 samples were obtained in each tumor from multiple trajectories and serial biopsies. Following our specific institutional protocol for any stereotactic biopsy procedure,[32] we used the site of higher MET uptake as the target of the biopsy. The CBV data were not used for the stereotactic planning. The target was transferred on the coregistered conventional MR images on which the trajectories were defined. Along each trajectory, 1 to 4 samples were taken at 1-cm intervals. The number of biopsy samples in each case was defined by the surgeon depending on the size and the location of the lesion (Fig 1*A–D*). The stereotactic coordinates of each sample were recorded during the surgical procedure to be used in subsequent analysis. Each biopsy was approximately 1 cm long with a diameter of 1 mm. Histopathologic examination of the samples was done in parallel by 2 experienced neuropathologists based on hematoxylin-eosin (H&E) coloration. They applied a semiquantitative evaluation of the samples (see below) and reached a consensus for all 65 samples used in this analysis. Each sample was first categorized as "peritumoral tissue" if there was no identified tumor cell within the sample, as "infiltrated tissue" if infiltrating tumor cells could be identified within brain tissue, or as "bulk tumor" if the tissue consisted only of tumor cells. Then, a semiquantitative analysis of histologic features was applied to each sample for: mitotic activity, endothelial cell proliferation, cellular pleomorphism, and tumor necrosis. A binary scale (1 = absent and 2 = present) was used. Mitotic activity was based on the presence or absence of mitosis. Tumor necrosis was characterized as pseudopalisading tumor cells around small zones of necrosis. All samples were then categorized on a scale ranging from a semiquantitative score of malignancy of 1 (absence of the above histologic features) to 5 (presence of all the above histologic features).

For each patient, the final histologic diagnosis was based on both H&E and routine immunohistologic evaluation using glial fibrillary acidic protein, vimentine, P-53 and Ki-67 antibodies. Tumors were graded according to the World Health Organization (WHO) classification.[1]

Image Postprocessing

The MR perfusion images were transferred to a commercial workstation (Easyvision; Philips Medical Systems) for postprocessing. The principles for the use of contrast agents to estimate perfusion have been described previously.[33-36] The relative CBV or CBV ratio is usually calculated by dividing the measured CBV in the lesion by CBV measured in the contralateral normal-appearing white matter.

CBV maps and PET images have been coregistered to 3DT1-weighted images using the normalized mutual information-based method[37,38] as implemented in the software package Statistical Parametric Mapping (SPM, University College, London, UK). For both 3DT1-weighted images and dynamic susceptibility-weighted contrast-enhanced MR images, the same FOV was chosen to facilitate the coregistration process despite the difference in voxel size. For coregistration between 3DT1-weighted images and PET images, data from the stereotactic frame were used to provide a more accurate result.

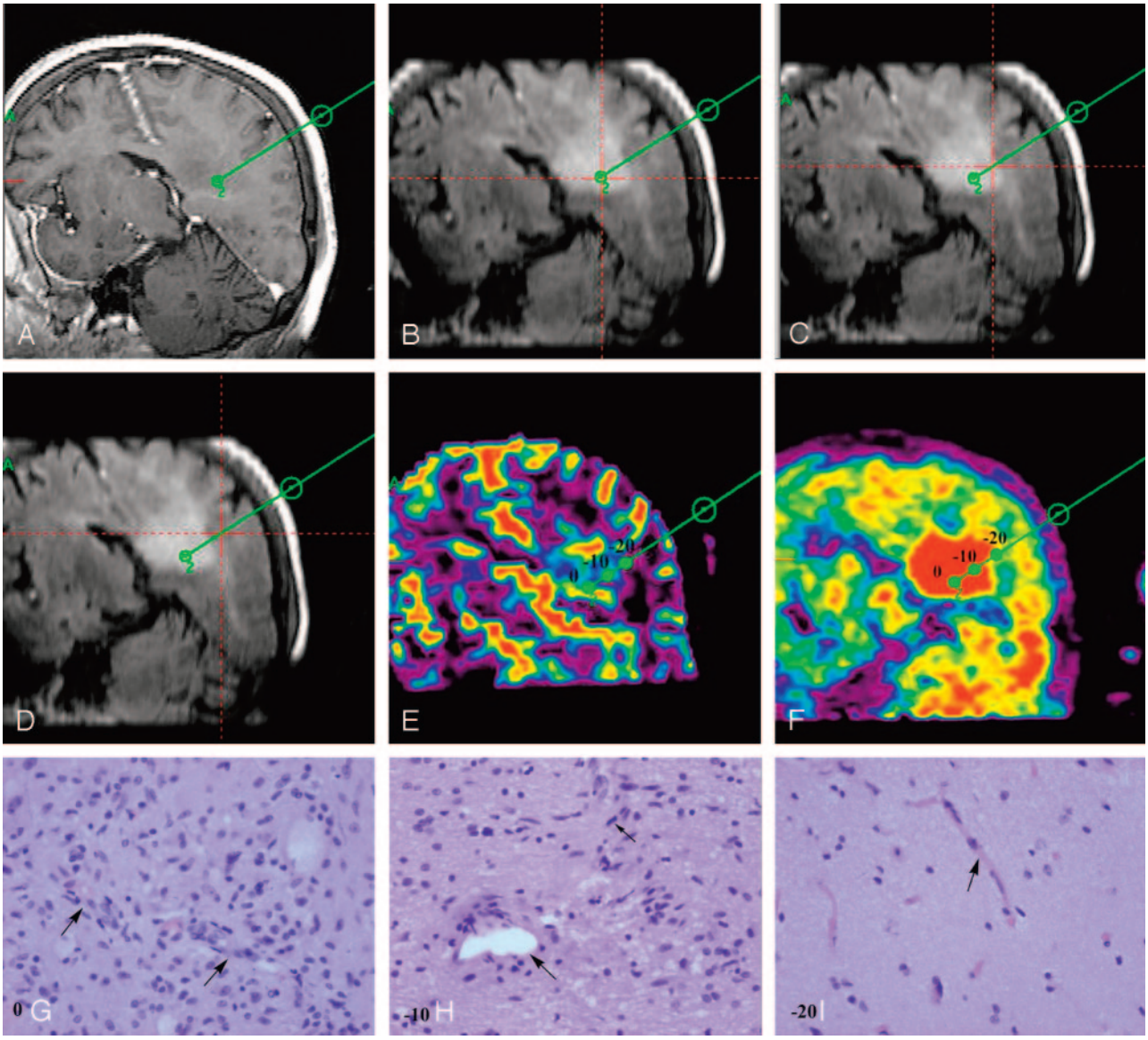

Fig 1. Image processing in the case of a 67-year-old woman with left parietal mass lesion corresponding to a low-grade astrocytoma (patient 7).

A, One of the 3 biopsy trajectories (trajectory 2) is projected into 3DT1-weighted image (TE, 20 ms; TR, 4.6 ms; flip angle, 25°; section thickness, 1.3 mm) with contrast. Note that the lesion is not enhancing.

B–D, On coregistered FLAIR images (TR, 6500 ms; TE, 150 ms; TI, 2200 ms), the lesion is better defined as an area of high signal intensity. Biopsy trajectory 2 is shown, and the point at which the red lines cross shows the area of biopsy at the target (*B*) and the 2 other samples at 1 (*C*) and 2 (*D*) cm from the target.

E-F, The position of the 3 biopsy areas at the target (0) as well as at 1 cm from the target (−10) and at 2 cm from the target (−20) are shown on both the coregistered CBV map (*E*) and the PET-MET image (*F*).

G–I, Photomicrographs (H&E coloration; original magnification, 400×) show the corresponding histologic characteristics of each biopsy specimen. The biopsy specimen from the target (0) corresponded to "bulk tumor" (*G*) where vessels with endothelial cell proliferation can be identified (*arrows*). The biopsy specimen from point (−10) corresponded to "infiltrated tissue" (*H*) where 1 mitosis (*small arrow*) and 1 vessel without endothelial cell proliferation (*large arrow*) are identified. The biopsy specimen from point (−20) corresponded to "peritumoral tissue" (*I*), where no tumor cell could be identified and vessels show a normal shape (*arrow*).

Previously recorded coordinates of each biopsy site could be retrospectively localized on the 3DT1 images on the Elekta workstation that was used for biopsy planning. Each biopsy site localized on 3DT1 images was found on coregistered axial CBV maps and PET images (Fig 1*E*, -*F*). The average signal intensity was computed in regions of interest (ROIs) of 25–32 mm^2 located at the biopsy site with the use of MRIcro software (available at http://www.sph.sc.edu/comd/rorden/mricro.html).[39] The size of the ROI was chosen to take into account the length of the biopsy specimen, the variable angles of the trajectory relative to the imaging axial plane, and the global error of the stereotactic biopsy method. A single observer measured both CBV and MET uptake values. Because the position of each ROI on CBV maps and PET images was given by the stereotactic coordinates of the biopsy site on the coregistered images, the placement of ROIs was not observer-dependent. In each patient, a single ROI was also placed in the contralateral normal-appearing white matter of the frontal or parietal lobe in both CBV maps and PET images. This ROI was large to minimize the variability of the reference value (600 to 1200 mm^2) and of irregular shape to better exclude cortical gray matter. Values in the white matter ROI were used to calculate CBV and MET uptake ratios. All further analyses made use of these normalized data.

Patient population						
Patient No	Age (years)	Sex	Histologic Diagnosis	Histologic Grade	Location	Number of Biopsy Specimens
1	26	F	PA	1	R cerebellum	4
2	25	F	LA	2	L temporal	3
3	55	F	LA	2	R frontoparietal	4
4	39	F	LA	2	R frontal	2
5	19	M	LA	2	R frontotemporal	11
6	78	F	LA	2	R temporal	3
7	67	F	LA	2	L parietal	8
8	47	M	O	2	L frontal	3
9	19	M	AA	3	L frontoparietal	9
10	33	M	AA	3	L temporoparietal	3
11	39	F	O	3	L temporoparietal	3
12	50	M	GB	4	R parietal	3
13	58	M	GB	4	L temporal	5
14	39	M	GB	4	Brain stem	4

Note:—PA indicates pilocytic astrocytoma; LA, low-grade astrocytoma; O, oligodendroglioma; AA, anaplastic astrocytoma; GB, glioblastoma; L, left; R, right.

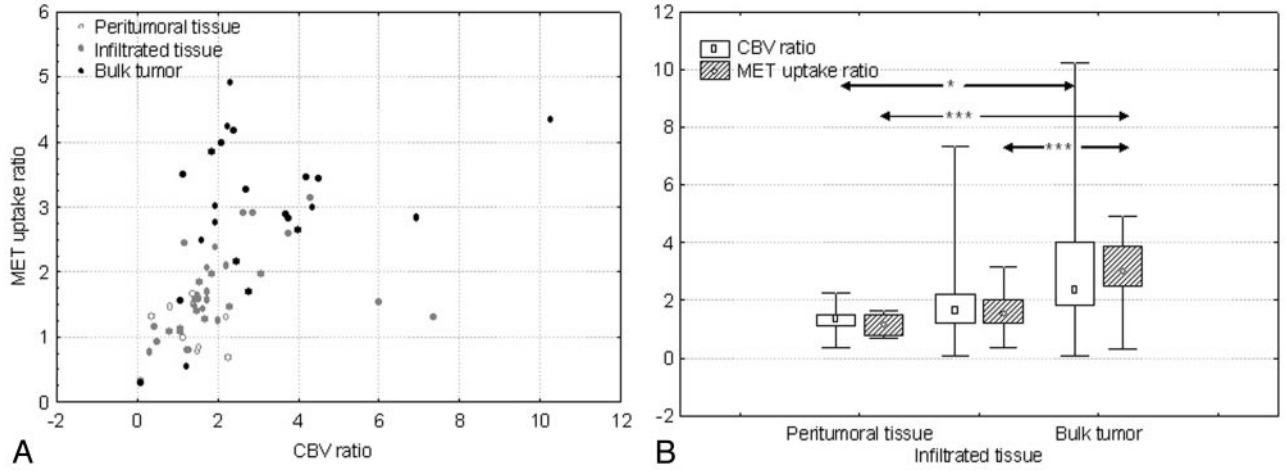

Fig 2. *A,* Scatterplot shows significant positive correlation between CBV ratios and MET uptake ratios ($r = 0.65$, $P < .001$). Measurements corresponding to "peritumoral tissue," "infiltrated tissue," and "bulk tumor" can also be identified.

B, Graph shows the relation between both CBV and MET uptake ratios and the histologic categorization of samples as "peritumoral tissue" ($n = 10$), "infiltrated tissue" ($n = 32$), and "bulk tumor" ($n = 23$). Median values increase significantly from "peritumoral tissue" to "bulk tumor" for both CBV and MET uptake ratios. The difference was also statistically significant between "infiltrated tissue" and "bulk tumor" for MET uptake ratios. Values are presented as minimum-maximum range (*whiskers*), 25th–75th percentile range (*box*), and median (*open symbols*). *, $P = .01$; ***, $P < .001$.

Statistical Analysis

Spearman rank-order correlation test was used to analyze the relationship between CBV ratios and MET uptake ratios. To compare CBV and MET uptake ratios with the different histopathologic features, nonparametric tests were used as follows: to compare CBV and MET uptake ratios with tissue infiltration by tumor cells, Kruskal-Wallis and Post Hoc tests were used; to compare CBV and MET uptake ratios with endothelial cell proliferation, mitotic activity, cellular pleomorphism, and tumor necrosis (2 classes), the Mann-Whitney test was used. A P value less than or equal to .01 was considered statistically significant. Receiver operating characteristic analysis was used to find the best cutoff threshold for both CBV and MET-uptake ratios. Statistica software was used for statistical analyses (StatSoft, Tulsa, Okla).

Results

The table summarizes patient population, histologic diagnosis, and grade and location of each tumor as well as the number of biopsy samples obtained in each case. Among the 65 samples analyzed on H&E coloration, 10 corresponded to "peritumoral tissue," 32 samples corresponded to "infiltrated tissue," and 23 samples corresponded to "bulk tumor" (Fig 1*G–I*).

CBV ratios ranged between 0.08 and 10.24 ($n = 65$, median = 1.73), MET uptake ratios ranged between 0.30 and 4.91 ($n = 65$, median = 1.67). A positive correlation was found between CBV ratios and MET uptake ratios ($r = 0.65$, $P < .001$) (Fig 2*A*).

Both CBV ratios and MET uptake ratios increased from "peritumoral tissue" to "infiltrated tissue" and to "bulk tumor" (Fig 2*B*). Both CBV and MET uptake ratios were significantly higher in "bulk tumor" compared with "peritumoral tissue" (CBV, $P = .01$; MET uptake, $P < .001$). MET uptake was also significantly higher in "bulk tumor" compared with "infiltrated tissue" ($P < .001$), but the difference was not significant for CBV ratios ($P = .05$). Neither CBV nor MET uptake ratios were significantly different between "peritumoral tissue" and "infiltrated tissue" ($P = .6$, $P = .26$, respectively) (Fig 2*B*).

Figure 3 compares the distribution of respective CBV ratios

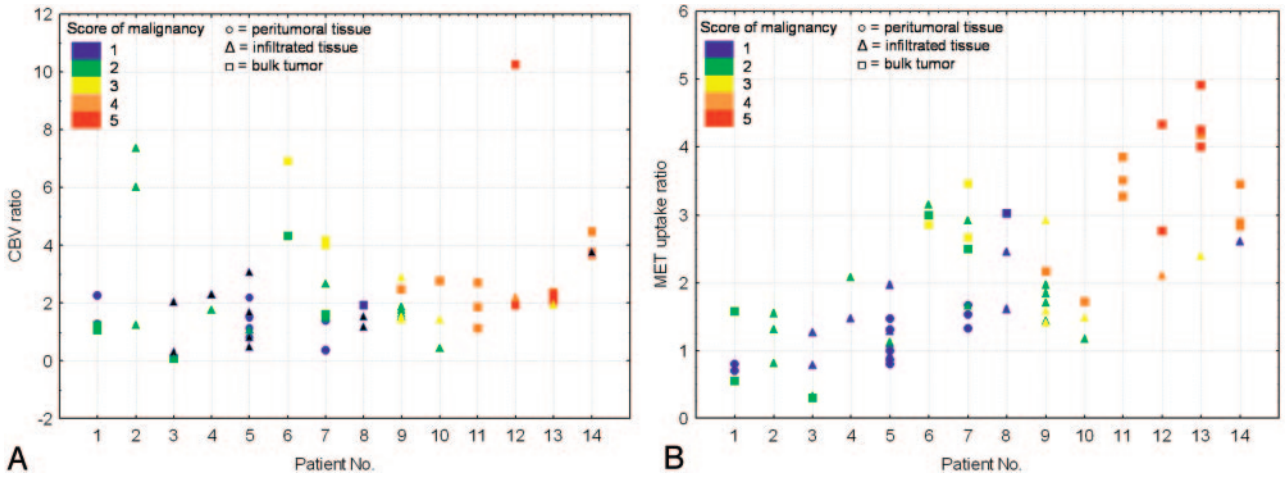

Fig 3. Graphs show the distribution of CBV ratios (*A*) and MET uptake ratios (*B*), respectively, in those patients with low-grade (patients 1–8) and or high-grade gliomas (patients 9–14). All samples are presented with different symbols depending on their category (○, "peritumoral tissue"; △, "infiltrated tissue"; □, "bulk tumor"), and different colors depending on their score on the semiquantitative scale of malignancy (*blue* = 1, *green* = 2, *yellow* = 3, *orange* = 4, *red* = 5; see text for details).

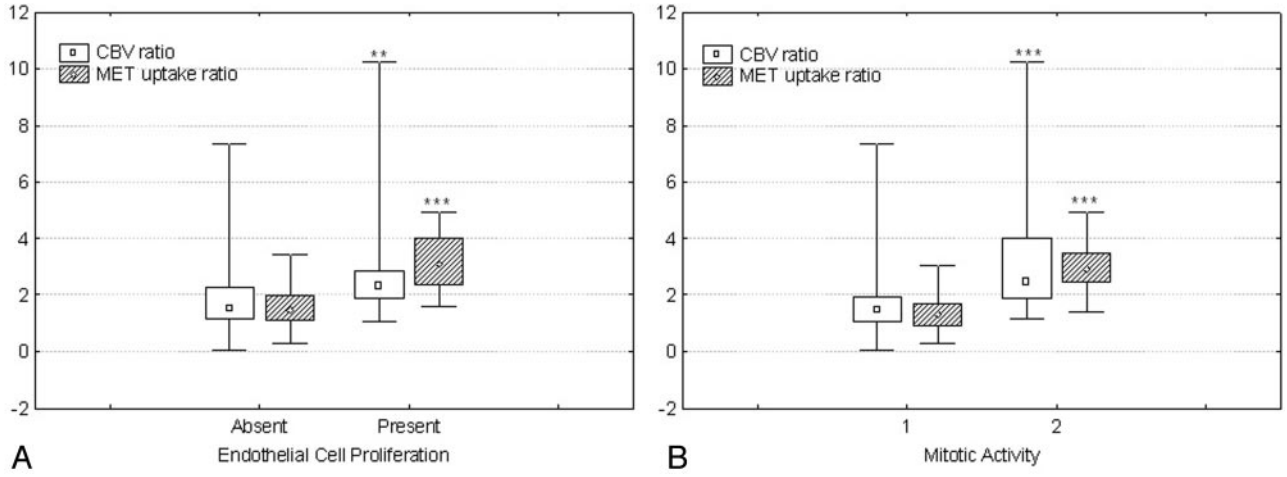

Fig 4. *A,* Graph shows the relation between both CBV and MET uptake ratios and the endothelial cell proliferation. The median values for both CBV and MET uptake ratios were statistically significantly higher in those areas with presence of endothelial cell proliferation ($n = 18$) compared with the areas without endothelial cell proliferation ($n = 47$).

B, Graph shows the relation between both CBV and MET uptake ratios and mitotic activity. The median values for both CBV and MET uptake ratios were statistically significantly higher in those areas with presence of mitosis ($n = 39$) compared with the areas without mitosis ($n = 26$). Values are presented as minimum-maximum range (*whiskers*), 25th–75th percentile range (*box*), and median (*open symbols*). **, $P = .01$; ***, $P < .001$.

and MET uptake ratios in each patient, in relation to tumor histologic diagnosis and grade. To determine the accuracy of CBV and MET uptake imaging for the detection of the area most representative of the actual tumor grade, we looked at the semiquantitative score of malignancy for the samples obtained at the site of highest CBV and MET uptake values. This question is most critical for the diagnosis of high-grade gliomas, which totally depends on the collection of representative malignant biopsy samples. The highest value of both CBV and MET uptake corresponded to the sample with the highest semiquantitative score for malignancy in 5 of 6 patients with high grade tumor (Fig 3). In the remaining patient of this group (patient 9), the semiquantitative score for malignancy was high, in accordance with the final histologic grade. By definition, in all low-grade gliomas, the semiquantitative score for malignancy remained low and relatively homogeneous. Highest CBV values corresponded to the sample with the highest score in 2 low-grade gliomas. This was the case in 3 patients for MET uptake values.

At the threshold of 1.5 for MET uptake ratios, tumor tissue (including both "bulk tumor" and "infiltrated tissue") could be detected with a sensitivity of 69% (38/55), specificity of 80% (8/10), positive predictive value of 93% (41/44), and negative predictive value of 33% (7/21). At the same threshold for CBV ratios, tumor tissue could be detected with a sensitivity of 69% (38/55), specificity of 70% (7/10), positive predictive value of 93% (38/41), and negative predictive value of 29% (7/24).

Both CBV and MET uptake ratios were found to be related to endothelial cell proliferation ($P < .01$, $P < .00001$) and mitotic activity ($P < .001$, $P < .0001$) (Fig 4*A*, -*B*). We found no significant relationship between necrosis and CBV or MET uptake in glioblastomas ($n = 12$, $P = .49$, $P = .17$). We limited this analysis to glioblastomas because necrosis is a cardinal feature of these tumors and has only been recorded in them. In the whole group of patients, the relation between either CBV ratio or MET uptake ratio and cellular pleomorphism was not statistically significant ($P = .2$, $P = .05$).

Discussion

In a previous study, Aronen et al[28] showed some correlation between tumor vascularity and tumor glucose metabolism based on maximum values of both CBV and glucose uptake in gliomas. Our study confirms a similar relationship between CBV and MET uptake in precise locations within gliomas. The correlation between CBV and MET uptake measurements reflects the idea that vascularity, which determines the value of CBV, is related to amino acid metabolism. Nevertheless, this correlation remains partial, indicating that these processes are differentially influenced by oncologic factors.

To better understand the relation between CBV and MET uptake, a local comparison with histologic analysis of the biopsy specimens was performed in the corresponding area. This comparison showed that both CBV and MET uptake measurements were related to the presence of tumor cells in brain tissue and both were significantly higher in "bulk tumor" than in "peritumoral tissue." MET uptake was also significantly higher in "bulk tumor" than in "infiltrated tissue," but CBV was not. MET uptake is dependent on metabolic processes at the *cellular level*. Thus, the PET signal intensity should be sensitive to the local tumor cell density, which is obviously higher in "bulk tumor" than in "infiltrated tissue." On the contrary, CBV is assumed to be a measure of capillary volume, a tumor characteristic defined at the *histologic level*. As such, it may vary less than MET uptake between "bulk tumor" and "infiltrated tissue."

Kracht et al[40] reported higher values of MET uptake in the infiltration area than in the solid tumor in a group of 5 low-grade astrocytomas. They linked this higher demand for amino acids in the peripheral areas of tumor infiltration to biologic stimulation related to processes such as cell adhesion, proteolytic remodeling, extracellular matrix synthesis, and activation by growth factors.[41,42] In contrast, the 6 low-grade astrocytomas of our series had MET uptake ratios that were statistically higher in "bulk tumor" compared with "infiltrated tissue." This discrepancy is probably related to a variable balance between effects of biologic stimulation and cell density, which both determine the signal intensity detected in each voxel of the images.

As a whole, the values of "peritumoral tissue" and "infiltrated tissue" were not significantly different, either for CBV or for MET uptake. In a practical prospect, however, it is noteworthy that at a threshold of 1.5, both CBV and MET uptake measurements well separated tumor tissue from "peritumoral tissue." Indeed, in a region where CBV or MET uptake values reach a threshold of 1.5, we can predict the presence of tumor cells with a high level of confidence (positive predictive value = 93%). This indicates that CBV, as well as MET uptake, provides valuable information for targeting diagnostic and therapeutic procedures. We calculated a sensitivity of 69% for both imaging techniques, which was less than that reported by Kracht et al[40] (87%) for MET uptake. However, this latter study, included nontumor lesions and nonglial tumors (lymphoma and metastasis) that have a different biologic behavior, particularly in terms of peripheral invasion. This difference in patient recruitment probably explains the higher sensitivity reported in that study.[40]

Low negative predictive values found for both CBV and MET uptake underlines the limits of both techniques in the total delineation of gliomas, which are characterized by their high propensity to infiltrate the surrounding brain tissues. Consequently, when part of the biopsy procedure aims to define the extension of the tumor process, further biopsy samples may be needed in areas with low CBV or MET uptake.

This study confirmed that both CBV and MET uptake values allow adequate targeting of stereotactic biopsy for the diagnosis of high-grade gliomas. Indeed, in all patients with high-grade tumors, the highest values of CBV and MET uptake corresponded to samples with high scores on a semiquantitative scale grouping histologic features of malignancy. In 5 of 6 cases, the highest values of CBV and MET uptake actually corresponded to the sample with the highest score on this semiquantitative scale (Fig 3).

Both CBV ratios and MET uptake ratios have been found to be related to at least 2 of the 4 histologic features used in grading gliomas: mitotic activity and endothelial cell proliferation. These relationships appeared more significant for MET uptake than for CBV ratios in all cases. Our results demonstrated a local relationship between MET uptake and mitotic activity that is in concordance with previous studies based on maximum MET uptake values.[16,17] The results of our study extend beyond previous results by demonstrating that within the tumor, the relationship holds true at a regional scale.

The fact that the increased amino acid uptake in gliomas is influenced by an increased transport mediated by type-L amino acid carriers located in the endothelial cell membrane probably gives an explanation for the relationship between MET uptake ratios and endothelial cell proliferation in our series of gliomas.[19,20]

The relationship between CBV and both endothelial proliferation and mitotic activity can be explained by the fact that in proliferating areas of tumor, neoangiogenesis is activated and produces vessels with endothelial cell proliferation.

In this study, we limited the histologic analysis to a semiquantification of the major grading features of gliomas. The present results prompt us to pursue analysis of histopathologic features in greater detail by using specific immunohistochemical markers of vascularity and proliferative activity. This is the subject of our ongoing investigations. In the present study, the immunohistologic evaluation available consisted of routine staining solely applied to part of the samples in each tumor case. Thus, it was not possible to conduct a correlative study between CBV and MET uptake measurements and the immunohistologic data obtained in each patient.

One particular aspect of our study is that the comparisons made considered each biopsy site independent from all other samples, even when obtained in the same patient. Therefore, the analyses of this study were conducted under the hypothesis that, in those highly regionally heterogeneous tumors, within- and between-patient variances of the biologic features are comparable. The number of specimens in each patient was not sufficient to statistically confirm the validity of this hypothesis, but the dispersion of the results in each patient supports the approach (Fig 3*A*, -*B*). Still, there may be some dependence between samples coming from the same patient because different areas of a single glioma probably share common biologic features. In further studies, a larger set of data points from a larger set of patients should permit multivariate regres-

sion analyses in search for relations between regional histology features and imaging characteristics.

Another limitation of our study was the heterogeneity of the patient groups in terms of glioma cell types. Indeed, we included astrocytic and oligodendrocytic glioma types that have different biologic behavior and clinical prognosis. This does not affect our general conclusions because the comparison was based on grading features that are common to the 2 types of tumors. Unfortunately, the small number of oligodendrogliomas in our series precludes an interesting comparison between "purely" astroglial and oligodendroglial tumors.

Conclusion

In conclusion, this study showed a regional positive correlation between CBV and MET uptake measurements in gliomas deploying a stereotactic coregistration method. These parameters were found to be significantly related to endothelial cell proliferation and mitotic activity of the corresponding biopsy specimens. As such, these imaging techniques may be used to analyze the heterogeneity of gliomas and to provide indices of local level of aggressiveness in these tumors. Both imaging techniques seem to be equivalent in the assessment of tumor infiltration.

References

1. Kleihues P, Burger PC, Scheithauer BW. **The new WHO classification of brain tumours.** *Brain Pathol* 1993;3:255–68
2. Russell D, Rubinstein L. **Tumours of central neuroepithelial origin.** In: Rubinstein LJ, ed. *Pathology of Tumours of the Nervous System*. 5th ed. Baltimore: Williams and Wilkins; 1989:83–350
3. Glantz MJ, Burger PC, Herndon JE 2nd, et al. **Influence of the type of surgery on the histologic diagnosis in patients with anaplastic gliomas.** *Neurology* 1991;41:1741–44
4. Levivier M, Goldman S, Pirotte B, et al. **Diagnostic yield of stereotactic brain biopsy guided by positron emission tomography with [^{18}F] fluorodeoxyglucose.** *J Neurosurg* 1995;82:445–52
5. Goldman S, Levivier M, Pirotte B, et al. **Regional methionine and glucose uptake in high-grade gliomas: a comparative study on PET-guided stereotactic biopsy.** *J Nucl Med* 1997;38:1459–62
6. Pirotte B, Goldman S, Massager N, et al. **Combined use of 18F-fluorodeoxyglucose and 11C-methionine in 45 positron emission tomography-guided stereotactic brain biopsies.** *J Neurosurg* 2004;101:476–83
7. Maia AC, Malheiros SM, da Rocha AJ, et al. **Stereotactic biopsy guidance in adults with supratentorial nonenhancing gliomas: role of perfusion-weighted magnetic resonance imaging.** *J Neurosurg* 2004;101:970–76
8. Derlon JM, Bourdet C, Bustany P, et al. **[^{11}C]L-methionine uptake in gliomas.** *Neurosurgery* 1989;25:720–28
9. Ogawa T, Shishido F, Kanno I, et al. **Cerebral glioma: evaluation with methionine PET.** *Radiology* 1993;186:45–53
10. Nuutinen J, Sonninen P, Lehikoinen P, et al. **Radiotherapy treatment planning and long-term follow-up with [^{11}C]methionine PET in patients with low-grade astrocytoma.** *Int J Radiat Oncol Biol Phys* 2000;48:43–52
11. De Witte O, Goldberg I, Wikler D, et al. **Positron emission tomography with injection of methionine as a prognostic factor in glioma.** *J Neurosurg* 2001;95:746–50
12. Ribom D, Eriksson A, Hartman M, et al. **Positron emission tomography (11)C-methionine and survival in patients with low-grade gliomas.** *Cancer* 2001;92:1541–549
13. Braun V, Dempf S, Weller R, et al. **Cranial neuronavigation with direct integration of ^{11}C methionine positron emission tomography (PET) data – results of a pilot study in 32 surgical cases.** *Acta Neurochir (Wien)* 2002;144:777–82
14. Levivier M, Massager N, Wikler D, et al. **Use of stereotactic PET images in dosimetry planning of radiosurgery for brain tumors: clinical experience and proposed classification.** *J Nucl Med* 2004;45:1146–54
15. Langen KJ, Muhlensiepen H, Holschbach M, et al. **Transport mechanisms of 3-[^{123}I]iodo-alpha-methyl-L-tyrosine in a human glioma cell line: comparison with [^{3}H]methyl]-L-methionine.** *J Nucl Med* 2000;41:1250–55
16. Chung JK, Kim YK, Kim SK, et al. **Usefulness of 11C-methionine PET in the evaluation of brain lesions that are hypo- or isometabolic on 18F-FDG PET.** *Eur J Nucl Med Mol Imaging* 2002;29:176–82
17. Sato N, Suzuki M, Kuwata N, et al. **Evaluation of the malignancy of glioma using 11C-methionine positron emission tomography and proliferating cell nuclear antigen staining.** *Neurosurg Rev* 1999;22:210–14
18. Kracht LW, Friese M, Herholz K, et al. **Methyl-[^{11}C]-l-methionine uptake as measured by positron emission tomography correlates to microvessel density in patients with glioma.** *Eur J Nucl Med Mol Imaging* 2003;30:868–73
19. Wienhard K, Herholz K, Coenen HH, et al. **Increased amino acid transport into brain tumors measured by PET of L-(2-^{18}F) fluorotyrosine.** *J Nucl Med* 1991;32:1338–46
20. Heiss P, Mayer S, Herz M, et al. **Investigation of transport mechanism and uptake kinetics of O-(2-[^{18}F]fluoroethyl)-L-tyrosine in vitro and in vivo.** *J Nucl Med* 1999;40:1367–73
21. Knopp EA, Cha S, Johnson G, et al. **Glial neoplasms: dynamic contrast-enhanced T2*-weighted MR imaging.** *Radiology* 1999;211:791–98
22. Law M, Yang S, Wang H, et al. **Glioma grading: sensitivity, specificity, and predictive values of perfusion MR imaging and proton MR spectroscopic imaging compared with conventional MR imaging.** *AJNR Am J Neuroradiol* 2003;24:1989–98
23. Lev MH, Ozsunar Y, Henson JW, et al. **Glial tumor grading and outcome prediction using dynamic spin-echo MR susceptibility mapping compared with conventional contrast-enhanced MR: confounding effect of elevated rCBV of oligodendrogliomas.** *AJNR Am J Neuroradiol* 2004;25:214–21
24. Aronen HJ, Gazit IE, Louis DN, et al. **Cerebral blood volume maps of gliomas: comparison with tumor grade and histologic findings.** *Radiology* 1994;191:41–51
25. Sugahara T, Korogi Y, Kochi M, et al. **Correlation of MR imaging-determined cerebral blood volume maps with histologic and angiographic determination of vascularity of gliomas.** *AJR Am J Roentgenol* 1998;171:1479–86
26. Cha S, Johnson G, Wadghiri YZ, et al. **Dynamic, contrast-enhanced perfusion MRI in mouse gliomas: correlation with histopathology.** *Magn Reson Med* 2003;49:848–55
27. Maia AC Jr., Malheiros SM, da Rocha AJ, et al. **MR cerebral blood volume maps correlated with vascular endothelial growth factor expression and tumor grade in nonenhancing gliomas.** *AJNR Am J Neuroradiol* 2005;26:777–83
28. Aronen HJ, Pardo FS, Kennedy DN, et al. **High microvascular blood volume is associated with high glucose uptake and tumor angiogenesis in human gliomas.** *Clin Cancer Res* 2000;6:2189–200
29. Van Gelderen P, Ramsey NF, Liu G, et al. **Three-dimensional functional magnetic resonance imaging of human brain on a clinical 1.5-T scanner.** *Proc Natl Acad Sci U S A* 1995;92:6906–10
30. Van Gelderen P, Grandin C, Petrella JR, et al. **Rapid three-dimensional MR imaging method for tracking a bolus of contrast agent through the brain.** *Radiology* 2000;216:603–08
31. Comar D, Cartron J, Maziere M, et al. **Labeling and metabolism of methionine-methyl-^{11}C.** *Eur J Nucl Med* 1976;1:11–14
32. Pirotte B, Goldman S, Massager N, et al. **Combined use of 18F-fluorodeoxyglucose and ^{11}C-methionine in 45 positron emission tomography-guided stereotactic brain biopsies.** *J Neurosurg* 2004;101:476–83
33. Rosen BR, Belliveau JW, Vevea JM, et al. **Perfusion imaging with NMR contrast agents.** *Magn Reson Med* 1990;14:249–65
34. Weisskoff RM, Zuo CS, Boxerman JL, et al. **Microscopic susceptibility variation and transverse relaxation: theory and experiment.** *Magn Reson Med* 1994;31:601–10
35. Weisskoff RM, Belliveau JW, Kwong K, et al. **Functional MR imaging of capillary hemodynamics.** In: Potchen E, ed. *Magnetic Resonance Angiography: Concepts and Applications.* St Louis: Mosby; 1993:473–84
36. Weisskoff RM, Rosen BR. **Noninvasive determination of regional cerebral blood flow in rats using dynamic imaging with Gd(DTPA).** *Magn Reson Med* 1992;25:211–12
37. Maes F, Collignon A, Vandermeulen D, et al. **Multimodality image registration by maximization of mutual information.** *IEEE Trans Med Imaging* 1997;16:187–98
38. Studholme C, Hill DLG, Hawkes DJ. **A normalized entropy measure of 3-D medical image alignment.** In: Hanson KM, ed. *Proceedings SPIE: the International Society for Optical Engineering. Medical Imaging 1998: Image Processing* 1998;3338:132–43
39. Rorden C, Brett M. **Stereotaxic display of brain lesions.** *Behav Neurol* 2000;12:191–200
40. Kracht LW, Miletic H, Busch S, et al. **Delineation of brain tumor extent with [^{11}C]L-methionine positron emission tomography: local comparison with stereotactic histopathology.** *Clin Cancer Res* 2004;10:7163–170
41. Rao JS. **Molecular mechanisms of glioma invasiveness: the role of proteases.** *Nat Rev Cancer* 2003;3:489–501
42. Tysnes BB, Mahesparan R. **Biological mechanisms of glioma invasion and potential therapeutic targets.** *J Neurooncol* 2001;53:129–47